

Particle acceleration, magnetization and radiation in relativistic shocks

Evgeny V. Derishev¹ and Tsvi Piran²

¹*Institute of Applied Physics, Russian Academy of Science, 46 Ulyanov Street, 603950 Nizhny Novgorod, Russia*

²*Racah Institute for Physics, The Hebrew University, Jerusalem, 91904, Israel*

Accepted XXX. Received YYY; in original form ZZZ

ABSTRACT

The mechanisms of particle acceleration and radiation, as well as magnetic field build up and decay in relativistic collisionless shocks are open questions with important implications to various phenomena in high energy astrophysics. While the Weibel instability is possibly responsible for magnetic field build up and diffusive shock acceleration is a model for acceleration, both have problems and current PIC simulations show that particles are accelerated only under special conditions and the magnetic field decays on a very short length scale. We present here a novel model for the structure and the emission of highly relativistic collisionless shocks. The model takes into account (and is based on) non-local energy and momentum transport across the shock front via emission and absorption of high-energy photons. This leads to a pre-acceleration of the fluid and pre-amplification of the magnetic fields in the upstream region. Both have drastic implications on the shock structure. The model explains the persistence of the shock generated magnetic field at large distances from the shock front. The dissipation of this magnetic field results in a continuous particle acceleration within the downstream region. A unique feature of the model is the existence of an “attractor”, toward which any shock will evolve. The model is applicable to any relativistic shock, but its distinctive features show up only for sufficiently large compactness. We demonstrate that prompt and afterglow Gamma-Ray Bursts’ shocks satisfy the relevant conditions and we compare their observations with the predictions of the model.

Key words: shock waves – acceleration of particles – radiation mechanisms: non-thermal – gamma-ray burst: general

1 INTRODUCTION

Relativistic outflows are ubiquitous in extreme astrophysical phenomena. Specifically, they arise in Gamma-Ray Bursts (GRBs), Active Galactic Nuclei (AGNs) and microquasars. Emission from such outflows originates at large distances from the central engine driving the outflow, most likely due to relativistic collisionless shocks that take place either within the outflows (internal shocks) or at the interface with surrounding medium (external shocks). According to the standard picture the shocks amplify magnetic fields and accelerate particles and these emit the observed radiation. The magnetic field energy density and the electrons’ energy density are characterized by equipartition parameters (typically assumed to be not much smaller than unity) that relate these energy to the total energy in the downstream.

While synchrotron emission characterized by such parameters works rather well in some cases (e.g. GRB afterglow) both observational and theoretical problems arise. Within GRB prompt emission this model is inconsistent

with the hard low energy spectrum observed at times [Cohen et al. \(1997\)](#); [Preece et al. \(1998\)](#); [Ghisellini et al. \(2000\)](#); [Gruber et al. \(2014\)](#). The apparent lack of high-energy inverse Compton (IC) component [Ackermann et al. \(2013\)](#) is also a puzzle.

On the theoretical side it was expected that the magnetic field at the front is comparable to the equipartition value: even if there is no field in the upstream, it will be generated through the Weibel instability. This was predicted theoretically [Moiseev & Sagdeev \(1963\)](#); [Medvedev & Loeb \(1999\)](#) and later confirmed by numerical simulations [Spitkovsky \(2008a\)](#). However, these Particle-in-cell (PIC) simulations indicate (in accord with early semi-analytic considerations [Gruzinov \(2001\)](#)), that the generated magnetic field decays rather quickly on the scale of the downstream skin depth. It is a matter of debate, how strong could be the magnetic field in the downstream far away from the shock front. Lacking a strong magnetic field downstream it is unclear how can this region radiate. Additionally, it is expected that particles are accelerated in collisionless shocks via the

Diffusive Shock Acceleration (DSA) mechanism [Spitkovsky \(2008b\)](#). However the same PIC simulations show that while DSA operates well if there is no magnetic field in the upstream or if the magnetic field is parallel to the shock normal, it becomes ineffective in the presence of even a modest perpendicular magnetic field (see [Sironi et al. \(2015\)](#) and references therein).

These recent theoretical developments question the ability of relativistic collisionless shocks to generate the observed emission and have led to numerous suggestions of alternative scenarios. For example, IC-modified thermal emission from a fireball [Rees & Mészáros \(2005\)](#); [Ryde \(2005\)](#); [Pe’er et al. \(2006\)](#); [Beloborodov \(2010\)](#); [Keren & Levinson \(2014\)](#), magnetic reconnection within a Poynting flux dominated outflow [Lyutikov & Blandford \(2003\)](#) and hadronic models (e.g. [Murase et al. \(2012\)](#)) have been proposed within the context of GRBs’ prompt emission. However these models have their own share of both phenomenological and theoretical problems. We present here a novel model of relativistic shocks that consistently treats both particle acceleration and radiation and resolves the above mentioned theoretical problems. The model is applicable to shocks with moderate magnetization, i.e., excluding Poynting-flux dominated outflows.

Other attempts to resolve these problems that have taken into account the influence of the shock on the upstream include: heating, pre-acceleration, build-up and distortion of the magnetic field, and possibly changes in the composition. Generally speaking there are two classes of such shock modification models. The first includes energy and momentum transport by fast particles or waves that propagate ahead of the shock front (see, e.g., [Eichler \(1979\)](#); [Blandford \(1980\)](#); [Bell \(2004\)](#); [Milosavljević & Nakar \(2006\)](#); [Medvedev & Zakutnyaya \(2009\)](#)). Another option, is electron-positron pair production in the upstream. This latter possibility has been suggested to arise if enough photons are backscattered by the surrounding matter. These backscattered photons annihilate some of the similar-energy outgoing photons (see, e.g., [Thompson & Madau \(2000\)](#); [Beloborodov \(2002\)](#)) creating pairs. For sufficiently large external scattering this leads to a runaway increase of pair density in the upstream modifying its structure. This is a non-local mechanism and, if it works, it always becomes the dominant one. However it depends critically on the scattering opacity of the external medium and this limits its applicability to external shock in some GRBs.

We propose here a different modification of the shock model. We suggest that “intrinsic” annihilation of outgoing high-energy and low-energy photons will also create pairs in the upstream and modifies this region. The key difference between this and the “standard” pair-loading scenario is that the pair-creation is “intrinsic”, i.e. it does not involve scattering by an external medium. As such the process is generic and will take place in any relativistic shock. However, now a source of high-energy photons in the downstream is needed. These high-energy photons arise due to inverse Compton scattering. In this case the length scale for the feedback between the downstream and upstream regions is set by the parameters of the shock. This allows for self-tuning of the shock structure (including self-consistent build up and decay of the magnetic field, as discussed later). As this is a long range process the modification of the upstream takes place on a much longer scale than the modification that arises

from fast particles that are moving ahead of the shock front creating an important long range structure in the magnetic field.

A second key idea in our model is the modification of the magnetic field by the pairs. The pairs that are produced in the upstream form an anisotropic lepton distribution which, in turn, leads to a pre-amplification of the magnetic field. This pre-amplification results in long wavelength modes. The magnetic field, which is further amplified at the shock front itself, decays in the downstream on a scale much larger than the skin depth in the downstream region. This picture is in conflict with PIC simulations that show a rapid decay of the magnetic field (e.g., [Sironi et al. \(2015\)](#)). However current PIC simulations don’t include the long-range momentum exchange processes discussed here. This process is mediated by high energy photons that are produced in the downstream and absorbed creating pairs in the upstream. Hence these PIC simulations cannot capture this feature of our model.

The energy released by the dissipating magnetic field is inevitably transferred to charged particles and then to synchrotron and inverse Compton radiation. The local distribution function of the leptons (and hence the local spectrum) is controlled by the magnetic field dissipation rate and it evolves together with the magnetic field as the shocked plasma advected downstream. Compared to the standard one-zone synchrotron shock model [Mészáros & Rees \(1997\)](#); [Sari et al. \(1998\)](#), this allows for additional flexibility in the emerging spectra [Derishev \(2007\)](#). This also leads to a similar length scale for the magnetic field decay, particle acceleration, and the radiative cooling. Thus this model does not suffer from incommensurability of the magnetic field decay and radiative cooling scales (in our model they appear to be approximately equal).

In order to avoid confusion let us explicitly list the key differences of our model from the pair loading scenario [Thompson & Madau \(2000\)](#); [Beloborodov \(2002\)](#), mentioned above. To distinguish between the two we denote this model as “external” pair loading scenario while the pair loading in our model is “intrinsic”. In the external pair loading scenario the target photons are outgoing (\sim MeV) photons that have been reflected by the surrounding matter. These reflected photons annihilate outgoing (also \sim MeV) photons. The resulting pairs have a small Lorentz factor relative to the lab frame. In our intrinsic model, pair production takes place between high-energy (IC) photons and low-energy synchrotron ones that are both moving forward in the lab frame. The pairs are highly relativistic and beamed in the lab frame. The number of pairs created does not depend on reflection from the external medium. Instead it is self-tuned to fit the shock’s energy release.

An extension of the external pair loading scenario suggests that the pairs may also influence the magnetic field in the upstream ([Ramirez-Ruiz et al. \(2007\)](#)). However, the delay between the onset of pair loading and arrival of the shock front is set by the shock propagation timescale. This scale is independent and much larger than the intrinsic shock timescales, especially the magnetic damping timescale. Thus, any magnetic turbulence generated in the upstream by these pairs is damped and will have a very limited effect on the magnetic field at the shock front. In contrast, in our intrinsic model the upstream modification

scale is controlled by the upstream absorption timescale, which in our model is proportional to the downstream cooling timescale (as explained in the paper), and it controls the magnetic damping timescale so all scales vary in the same way.

The only way to fully explore our model is through numerical PIC simulations that include this long-range energy and momentum exchange between the downstream and the upstream. However, a simplified phenomenological version of the model can yield important analytic insights towards general features of relativistic shocks and their broad-band spectra. We describe and analyze such a model here. In order to advance with an analytic solution, we introduce several assumptions. The assumptions are not required by the model in a general sense; it works just as well when they are not satisfied. But they greatly reduce the model's complexity and yet are reasonable for the shocks expected in GRBs and in AGNs. In particular we analyze a simplified, phenomenological model, in which we assume the magnetic field decay law rather than calculate it self-consistently. This keeps the problem tractable and enables us to obtain analytic results regarding the structure of relativistic shocks and their emission.

When applying these ideas to GRBs, it should be noted that the mechanisms behind the prompt and the afterglow emission may be different. In the following we don't attempt to provide a complete phenomenological solution to either prompt or afterglow emission. In fact the current status of the development of the model, as exposed here, is probably not suitable for this task as yet. Instead, we point out in numerous places in the text, the consistency of our estimates with typical parameters, believed to be applicable to both internal and external shocks in GRBs. While the full observational implications of the model are not clear yet we explore various pros and cons of this model when confronted with GRB observations in the concluding paragraph.

We begin, in 2, with a step-by-step description of model's physics. In 3 we discuss the spatial scales relevant to the problem and their hierarchy. Each of the model's building blocks is then substantiated and discussed in greater detail in one of the subsequent sections. We conclude in 12 summarizing the basic features of this model and some of its observational implications.

2 MODEL'S FRAMEWORK

Shock structure: We begin with an outline of the physical framework of the model. We consider an ultra relativistic shock propagating into a surrounding cold region. The shock is divided into three regions, denoted in Fig. 1 by Latin numbers. The downstream region (I), which we consider as the primary source of emission, is filled with hot compressed plasma, where both electrons (with a possible admixture of positrons) and protons (or ions more generally) are highly relativistic. The magnetic field gradually decays in this region and it is this decay that heats the particles there. Energized electrons then emit both synchrotron and high-energy inverse Compton radiation. Absorbed high energy photons from the downstream lead to pre-acceleration at the upstream region (II) and to pre-amplification of the magnetic field there. The magnetic field is further amplified

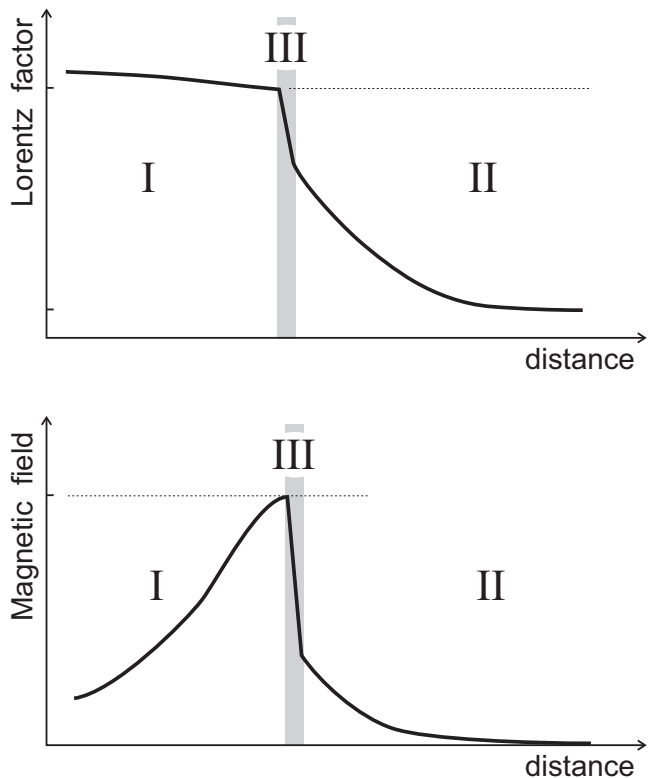


Figure 1. A schematic description of the shock structure with three zones (downstream - I, pre-accelerated upstream - II and the shock front - III). Shown are the bulk Lorentz factor in the laboratory frame (upper panel) and the comoving-frame magnetic field strength (lower panel) as functions of distance. The distance is measured along the shock normal and counter to the shock velocity. The shock moves to the right.

at the shock front (III) and particles are boosted once they cross it. We do not resolve the front and we consider it as an infinitely thin surface. Unlike the standard shock model in which both particle acceleration and magnetic field amplification take place in this front, its role is reduced here to the amplification of the magnetic field.

We assume that the total thickness of the structure, shown in Fig. 1, is much less than the shock curvature radius, so that the system is essentially one-dimensional. This curvature radius, however, enters as a parameter that determines the timescale for photon escape and hence the radiation density in the emitting regions.

Emission and absorption of high-energy photons: The resulting radiation field is produced within the different components of the shock either via synchrotron radiation or via IC. Both originate from the populations of relativistic electrons and positrons (whose number and the distribution function differ from one point to another). The luminosities of the synchrotron and IC emission are approximately equal when the shock is in the fast cooling regime or close to it. This claim is substantiated in Sect. 5.

The estimated energy of the radiating electrons is often close to the value, where the Klein-Nishina effect becomes important. In Sect. 9 we show that this is not a coincidence, but rather a natural result of shock parameters evolution. Under such conditions, absorption of the IC radiation inside the shock is important (see Sect. 5 for quantitative esti-

mates). Indeed, by definition at the Klein-Nishina cutoff the energy of the upscattered photons is just at the optimum for two-photon pair production with the low energy photons. As the cross-section for pair production is of the same order of the scattering cross-section. So, if cooling through IC emission is efficient, then two-photon absorption of the produced radiation is also efficient.

Upstream pre-acceleration: Some of the high-energy IC photons produced in the downstream region interact within the shock region with low-energy synchrotron photons and produce pairs. This strongly influences the shock's structure and shapes its evolution. This process links upstream to the downstream, so that the upstream is no longer casually disconnected from the downstream. This non-local energy and momentum exchange between the downstream and the upstream is the backbone of our model.

The secondary pairs transfer energy and momentum to the upstream, so that it starts accelerating long before the shock front arrives. As a result, the velocity jump across the shock front decreases, possibly to the extent that it becomes sub-relativistic, or even disappears if the pair loading is strong enough. At the same time, the downstream velocity relative to the shock front increases. The effect of upstream pre-acceleration is quantitatively analyzed in Sect. 6.

Energyization at shock crossing: The decrease in the shock front speed and the increase in the downstream velocity relative to the shock front act in accord to make diffusive shock acceleration less efficient. Hence, unlike the conventional shock acceleration model (see Piran (2004) for a review), we don't postulate acceleration of particles at the shock front. Instead, two other mechanisms maintain the population of energetic emitting particles.

Once the energetic pairs, which have been produced in the upstream cross the shock front, they are boosted by the Lorentz factor between the upstream and the shock front. Thus, the energy of such pairs exceeds the energy of the original photons that have produced them. This population of energetic electrons is the source of the next generation of photons that, in turn, will be again absorbed in the upstream producing even more energetic pairs. With each subsequent cycle, both the total and the individual energy of the particles involved into this process are multiplied by a large factor. This constitutes the converter acceleration mechanism Derishev et al. (2003); Stern (2003) that operates in every relativistic shock with a non-vanishing opacity for photon-photon interaction. Without special measures to counteract it, the converter acceleration is over-efficient and eventually it leads to depositing all the available energy into the highest energy pairs, resulting in a cascade spectrum that is very different from the observed one. In Sect. 7 we describe a self-regulating mechanism that keeps this process under control and limits it. The net result of the converter acceleration in our model is the formation of high-energy tail in the electron-positron distribution function. These high-energy electrons and positrons are injected into the downstream at the shock front and contain a sizeable, but not dominant, fraction of energy in radiating particles.

Magnetic field generation and decay: In addition, the continuous injection of pairs maintains anisotropic particle distribution in the upstream, which gradually builds up the magnetic field over a distance that is orders of magnitude larger than the plasma skin depth. The magnetic energy is

therefore channelled to large-scale modes, which grow slowly, but also survive for long time in the downstream. The spatial scale for the magnetic field growth and decay is set by the absorption length of the IC radiation and it is comparable to the shock's dynamical scale (the timescale of shock's expansion, measured in the comoving frame). The estimates of the magnetic field decay time, as well as its correlation length and magnitude are presented in Sect. 8.

The long range decay of the magnetic field is a key feature in our model. As was noted earlier, the assumption of slow magnetic field dissipation apparently contradicts results of PIC simulations. However, this contradiction does not prove that either our model is wrong or that the simulations are incorrect. Instead, the simulations deal with a different physical problem in which some of the crucial ingredients of our model are missing. In particular, the PIC simulations don't involve the radiation field and hence they miss the gradual pre-acceleration of the fluid and the gradual build up of the magnetic field in the upstream region. These processes arise from absorption of photons produced by the downstream in the upstream region. Put differently, the PIC simulations deal with an almost instantaneous build-up of the anisotropy in the particle distribution function that is followed by a rapid build up and a rapid decay of the magnetic field, whereas in our model the anisotropy is maintained by injection over a long range.

The longest available PIC simulations show that the magnetic field dissipation length increases (together with the field correlation length) as the particles gain energy at the shock and increase their mean free path Sironi et al. (2013). The lesson to be learned from the simulations is that the magnetic field decays over a length, which is roughly equal to its build-up length. In our model, due to the energy and momentum exchange via the photons, the build-up length is many orders of magnitude larger than the plasma skin depth. We expect the decay to follow suit.

Particle acceleration due to the magnetic field decay: The energy released from magnetic dissipation in the downstream heats the plasma and it is channelled to accelerated particles. This results in a distributed particle acceleration (heating) all over the downstream emitting region.

Once accelerated the electrons and positrons lose energy to synchrotron and inverse Compton radiation. We assume that radiative cooling is fast, so that the electrons and positrons emit locally the energy they receive from the dissipating magnetic field. The average electron's Lorentz factor is determined, in this case, by the local balance between energy gain and losses. The assumption of fast cooling is not a necessary ingredient of the model and it is done only in order to simplify the estimates carried out here.

We assume that the net effect of the heating and the radiative losses is to produce either a relativistic thermal distribution or a power law distribution with smoothed low-energy cut-off. These options are meant to deal with two opposite extremes: the first is for the case where heating occurs through a rapid succession of small energy gains, while the second corresponds to the case where heating results from rare leaps in energy, each one large compared to the average energy.

Electrons heated by magnetic dissipation in the downstream produce the bulk of the shock's emission. In Sect. 4 we analyze the evolution of electron distribution function

in the downstream. This evolution, as we will show, determines the spectral shape at frequencies below the synchrotron peak, whereas the peak itself is maintained by the process of pair production at the location, which corresponds to Comptonization at the verge of Klein-Nishina cutoff.

Pair loading in the downstream and self-tuning: If the shock starts with such parameters, that the IC radiation is produced in the Klein-Nishina regime, then the secondary pairs can easily outnumber the primary electrons. Since the heating power is fixed by the magnetic field decay, a larger number of radiating particles implies that an average particle becomes less energetic and produces less energetic IC photons, which are absorbed less efficiently. This feedback rapidly drives the shock's parameters to the point, where an average IC photon is just below the pair production threshold when interacting with the most abundant synchrotron photons. The opacity for IC radiation drops and so does the pair production rate. Thus, the pair production rate stabilizes at the level where it exactly resupplies the particle loss into the downstream. The resulting steady state represents an attractor solution that exists for a wide range of parameters. Interestingly, with reasonable parameters, this attractor solution yields peak photon energies that are in the range of observed peak energies for GRBs' emission. The self-tuning of relativistic shocks is discussed in Sect. 9.

The different radiation components: Overall there are three distinct emitting regions. The primary (most powerful) source of the synchrotron and IC radiation is the downstream region of decaying magnetic field. In Sect. 10 we calculate the spectrum of synchrotron emission from this region, but we do not discuss the spectrum of IC component in any detail. The most energetic pairs that were born upstream may have enough time to cool radiatively before reaching the shock front. These are responsible for formation of yet another, upstream, emission component.

In general, the spectra and temporal evolution of downstream and upstream emission are very different because of different bulk Lorentz factors, which, in addition, is not uniform across the upstream. Typically we expect the upstream emission component to be weak compared to the downstream one. However, this may change under certain conditions. As discussed in Sect. 5, the upstream intercepts a fair fraction of radiation released by the downstream, and potentially a part of this may be re-radiated by the upstream itself. Finally a third component is due to energetic leptons from the upstream that have been boosted while crossing the shock front and reached the downstream. There these pairs find themselves in strong magnetic field and quickly lose their energy, mostly through the synchrotron emission. This gives rise to a radiation component, which we call transitional since it is due to particles that transit from the upstream to the downstream and then radiate in the vicinity of the shock front. The contribution of the transitional emitting region to the synchrotron SED is a power-law tail at high energies, which is calculated in Sect. 11. Again, we don't calculate the spectrum of IC component in the transitional radiation, but note that it is of relatively smaller importance because of the Klein-Nishina cutoff.

3 LENGTH SCALES

At a relativistic shock, where two plasma flows meet and penetrate into each other, the magnetic field is generated via a Weibel-type instability. This process proceeds rather quickly, up to the length of the order of relativistic plasma skin depth (in the comoving frame)

$$l_s = \left(\frac{\Gamma m_p c^2}{4\pi e^2 n_p} \right)^{1/2} = \frac{1}{n_p} \left(\frac{e_t}{4\pi e^2} \right)^{1/2}, \quad (1)$$

where Γ is the shock Lorentz factor, m_p the proton (ion) mass, e the elementary charge, n_p the number density of protons, and $e_t = \Gamma m_p c^2 n_p$ the total energy density, both in the shock-comoving frame. For GRB external shocks, for example, the comoving length given by Eq. 1 is

$$l_s \simeq \frac{4 \times 10^5 \text{ cm}}{n_3^{1/2}}, \quad (2)$$

where n is the number density of ambient medium in the lab frame and the subscript x denotes a quantity in cgs units of 10^x . The density $n_3 \sim 1$ is typical for a wind from a Wolf-Rayet star at the distance of 10^{16} cm. The large-scale magnetic turbulence generated in the upstream slows down the Weibel instability and broadens the shock front, as discussed in Sect. 8, but its width remains many orders of magnitude smaller than any other spacial scale in the system.

Numerical PIC simulations show that the magnetic field initially takes up a substantial fraction of the shocked plasma energy density. It has a spacial scale of the order of l_s . As the plasma recedes from the shock front, the field's spacial scale increases and its strength decreases (see Sironi et al. (2015) and references therein). This results from rearrangement of the magnetic field lines and possibly from reconnection that generates strong local electric fields. Charged particle are accelerated when they randomly encounter these electric fields. In this way energy is transferred from the decaying magnetic field to the electrons and positrons. All relativistic particles of the same charge are energized on equal grounds, so that the non-radiating protons would receive (and waste) half of the magnetic decay energy, unless electrons and positrons greatly outnumber protons and take over energy expenditures. As we show later, our model fits the latter case. Since there is no reason for the electron distribution to differ from positron distribution, we will make no difference between electrons and positrons, and the name "electrons" hereafter denotes both.

We will characterize the length scale for the magnetic field dissipation, l_d , as

$$l_d = \lambda l_s, \quad (3)$$

where $\lambda \gg 1$ is the model parameter. Though the actual value of this parameter is unknown, it is likely very large, exceeding unity by many orders of magnitude. The decay length of the magnetic field is set up by the spatial scale of the currents rather than by the plasma skin depth. The low- k modes of the magnetic field generated in the upstream increase the correlation length of the downstream magnetic field and hence the decay length. Thus, the magnetic field decay length is determined by the length scale on which the IC photons are absorbed in the upstream,

$$l_{abs} = R/\Gamma\tau_c, \quad (4)$$

where $\tau_c \equiv \sigma_{\gamma\gamma} n_{ph} R/\Gamma$ is the optical depth, n_{ph} is the target photon number density and $\sigma_{\gamma\gamma}$ is the effective two-photon pair production cross section. To evaluate the absorption scale we will need to wait to section 10. Typically $l_c < l_{abs} \approx l_d$.

A third important scale is the electron cooling length. Moving into the downstream with a bulk velocity $\beta_d c$ (for an unmodified relativistic shock $\beta_d = 1/3$), the electrons cool over the distance

$$l_c = \frac{3\beta_d m_e c^2}{4\sigma_T \gamma (1+y) e_B}, \quad (5)$$

where m_e is the electron's rest mass and γ its Lorentz factor, σ_T is the Thomson cross-section, e_B the magnetic field energy density and y is the Compton parameter. It is convenient to define the average Compton parameter, \bar{y} :

$$(1+\bar{y}) \int_1^\infty \gamma^2 f_e d\gamma \equiv \int_1^\infty \gamma^2 (1+y) f_e d\gamma, \quad (6)$$

where $f_e(\gamma)$ is the electron distribution function. The actual value of \bar{y} turns out to be insensitive to the model details; normally \bar{y} is about a few. Numerically (for GRBs' external shocks), the cooling distance is

$$l_c \simeq \frac{5 \times 10^9}{\gamma_3 \Gamma_2^2 n_3 \epsilon_B} \text{ cm}, \quad (7)$$

where n is the number density of ambient medium in the lab frame and the magnetic equipartition parameter is defined as $\epsilon_B \equiv e_B/e_t$.

It is instructive to compare the cooling distance with the plasma skin depth:

$$\frac{l_s}{l_c} \simeq \frac{8}{9\beta_d} \gamma (1+y) \epsilon_B (4\pi r_e^3 n_p)^{1/2} \Gamma^{3/2} \left(\frac{m_p}{m_e} \right)^{3/2}, \quad (8)$$

where $r_e = e^2/(m_e c^2) \simeq 2.8 \times 10^{-13}$ cm is the classical electron radius. The shock-front width (roughly equal to the skin depth) is always orders of magnitude smaller than the cooling distance. For example, in GRBs' external shocks

$$\frac{l_s}{l_c} \sim 10^{-4} \gamma_3 \Gamma_2^2 n_3^{1/2} \epsilon_B. \quad (9)$$

A mildly relativistic shock would require densities typical for condensed matter to make these scales comparable. It makes possible modeling of radiatively efficient shocks in laboratory laser plasma.

We assume the following hierarchy of spacial scales:

$$l_s \ll l_c \ll l_d \leq R/\Gamma, \quad (10)$$

where R is the shock radius and R/Γ is the comoving shock scale. The right inequality ensures that the magnetic field transfers substantial part of its initial energy to particles, while the central one guarantees that the fast cooling approximation is adequate. The right inequality inevitably breaks down at some point in the course of the deceleration of an external shock, and the second one is more like $l_c \lesssim l_d$ when it comes to a self-consistent solution (we will elaborate on this in Sections 9 and 10).

4 DISTRIBUTION FUNCTION OF ELECTRONS IN THE DOWNSTREAM

When the decaying downstream magnetic field heats electrons and positrons, which are in the fast cooling regime,

their average energy is set by the local balance between the heating rate per unit volume and the average emissivity of the electrons. The former equals the decrease of magnetic field energy density in the case where electrons greatly outnumber protons and half of that otherwise¹, and the latter is determined by the shape of electron distribution over their energies. This shape depends on the amplitude distribution of kicks that the electrons receive when passing through the electric fields. As we do not explore the details of the dissipation process of the magnetic field, the corresponding statistic of kicks is unknown and some a priori assumption about the electron/positron distribution is necessary. Simple and reasonable choices are either relativistic thermal distribution

$$f_e(\gamma) = \frac{27}{2\gamma_0^3} \gamma^2 \exp(-3\gamma/\gamma_0) n_e, \quad (11)$$

or a power law distribution²

$$f_e(\gamma) = \frac{p(p-1)}{2} (C\gamma_0)^{p-1} \frac{\gamma^2}{(C\gamma_0 + \gamma)^{p+2}} n_e; \quad (12)$$

$$C = \frac{p-2}{3}, \quad p > 3.$$

For both distributions the mean electron energy is $\gamma_0 m_e c^2$. The bulk of synchrotron emission is due to electrons with $\gamma \sim (5/3)\gamma_0$ for the thermal distribution and $\gamma \sim (5(p-2)/3(p-3))\gamma_0$ for the power-law one.

The inequality (10) implies that the energy change due to adiabatic expansion or compression is negligible. Then, the equilibrium average Lorentz factor γ_0 varies with the distance from the shock front following the changes in the local energy density of the magnetic field and can be calculated from the balance between acceleration and losses:

$$\frac{4}{3} \sigma_T e_B \int_1^\infty \gamma^2 (1+y) f_e(\gamma, \gamma_0) d\gamma = -\beta_d \frac{\partial e_B}{\partial r}, \quad (13)$$

where r is the distance from the shock front. Substitutions from Eqs. (6) and one of (11), (12) result in

$$\frac{4}{3} \langle \gamma^2 \rangle \sigma_T n_e e_B (1+\bar{y}) = -\beta_d \frac{\partial e_B}{\partial r}. \quad (14)$$

The average of the Lorentz factor squared is $\langle \gamma^2 \rangle = (4/3)\gamma_0^2$ for the thermal distribution and $\langle \gamma^2 \rangle = (4(p-2)/3(p-3))\gamma_0^2$ for the power-law distribution. The function $\gamma_0(r)$, can be determined as soon as the magnetic field decay law $\partial e_B/\partial r$ is known. Most reasonably, γ_0 is a monotonically decreasing function of the distance from the shock and hence its value near the shock front determines the bulk properties of emission spectrum.

¹ Highly relativistic electrons and protons, having equal charge, should gain the same energy when accelerated in local electric fields, which result from the magnetic field dissipation.

² While smooth at γ_0 , this distribution is effectively similar to the truncated power-law with a minimal Lorentz factor, γ_{min} , commonly used in GRB modeling.

5 EMISSION AND ABSORPTION OF INVERSE COMPTON RADIATION

Equation 14 allows us to find the synchrotron emission coefficient

$$j = -\frac{\beta_d c}{4\pi(1+\bar{y})} \frac{\partial e_B}{\partial r} \quad (15)$$

and then the intensity of synchrotron radiation at the front of plane-parallel shock is

$$I(\theta) \simeq \frac{1}{\cos(\theta)} \int_0^\infty j \, dr \simeq \frac{\beta_d c e_B(0)}{4\pi(1+\bar{y}_0) \cos(\theta)}. \quad (16)$$

Here θ is the angle between shock normal and the line of sight. The first equality in Eq. (16) would be exact in the downstream frame assuming that the downstream velocity is constant, but in the shock-front frame it is approximate because the downstream is moving, although at a non-relativistic velocity, and the Doppler boosting makes beam pattern to appear anisotropic in the shock-front frame even if it is isotropic in the comoving frame.

According to Eq. (16), the intensity diverges as θ tends to $\pi/2$. This is an artifact of the plane geometry approximation. However, the shock has a finite curvature, so that the maximum intensity is limited. This can be taken into account by introducing the geometrical factor $\Lambda \simeq \ln(R/l_d/\Gamma)$. The approximate energy density of the synchrotron radiation at the shock front is

$$e_{sy} = \frac{2\pi\Lambda I(0)}{c} = -\frac{\Lambda\beta_d}{2} \int_0^\infty \frac{\partial e_B/\partial r}{1+\bar{y}} \, dr. \quad (17)$$

The energy density of radiation produced by a geometrically thin shock depends logarithmically on the distance from the shock front and hence can be considered constant. If, in addition, the Klein-Nishina cutoff does not appear near to a local SED maximum (usually it is the synchrotron SED maximum), then the fraction of the radiation density e_r that accounts for the inverse Compton losses is also nearly constant. Substituting in the above integral \bar{y} with e_r/e_B , and assuming $e_r = \text{const}$, we obtain

$$\frac{e_{sy}(0)}{e_B(0)} = \frac{\Lambda\beta_d}{2} \left[1 - \bar{y}_0 \ln \left(1 + \frac{1}{\bar{y}_0} \right) \right], \quad (18)$$

where the argument (0) stands for the shock front ($r = 0$) and $\bar{y}_0 = \bar{y}(0) \simeq e_r(0)/e_B(0)$.

Equation (18) can be solved for a number of special cases. The first (and trivial) possibility is that the bulk of synchrotron radiation is above the Klein-Nishina cutoff frequency. Then $y = 0$ by definition, and $e_{sy}(0)/e_B(0) = \Lambda\beta_d/2$. In the second case, the synchrotron radiation is scattered off electrons in the Thomson regime, while the scattering of the comptonized photons is suppressed by the Klein-Nishina effect. Then $e_{sy}(0)/e_B(0) = \bar{y}_0$. Since the geometrical factor is a few, a further approximation is not possible and Eq. (18) has to be solved numerically. The resulting values are $\bar{y}_0 = 0.28, 0.46, 0.65$ for $\Lambda = 3, 6, 10$ and $\beta_d = 1/3$.

Finally, it is possible that k times comptonized radiation is still below the Klein-Nishina cutoff, while the next comptonization step sends photons above the cutoff. Then one has to substitute $\bar{y}_0 = (e_{sy}(0)/e_B(0))^{k+1}$. The actual parameters in GRB shocks place them between the first and the second cases above. However, relativistic shocks are able to self-tune their parameters, as discussed in Sect. 9, so that

they tend towards the second case, with comptonization just approaching the Klein-Nishina regime. The self-tuning effect has limited capabilities and not every shock can pull its parameters to this optimum, but for the GRB shocks this is within reach.

Combination of large Compton y parameter and fast cooling at the same time means that the IC radiation, produced in the Klein-Nishina regime or close to it, will be strongly absorbed within the shock. The optical depth for photon-photon collisions is

$$\tau_c = \sigma_{\gamma\gamma} n_{ph} \frac{R}{\Gamma} = \sigma_{\gamma\gamma} \frac{R}{\Gamma} \frac{e_B(0)}{E_p}, \quad (19)$$

where n_{ph} is the target photon number density and $\sigma_{\gamma\gamma}$ the effective two-photon pair production cross section. Here we have assumed that all the magnetic energy is eventually radiated away and we have used the magnetic energy density, e_B , to estimate the radiation energy density. We have ignored the logarithmic increase of the radiation energy density close to the shock front. The conservative estimate (19) assumes that the most efficiently absorbing target photons are those at the peak of synchrotron SED. This holds only for sufficiently hard low-energy SED asymptotes, so that in some cases the actual optical depth may be larger.

The estimated value of the optical depth for GRBs' external shocks is

$$\tau_c \simeq 50 \sigma_{\gamma\gamma, -25} \epsilon_B R_{16} \Gamma_2^2 n_3 \frac{m_e c^2}{E_{p, lab}}, \quad (20)$$

where $E_{p, lab} = \Gamma E_p$ is the lab-frame synchrotron peak energy. For internal shocks, the optical depth is

$$\tau_c \simeq 100 \sigma_{\gamma\gamma, -25} \frac{L_{iso, 51}}{\Gamma_3^2 R_{13}} \frac{m_e c^2}{E_{p, lab}}, \quad (21)$$

where Γ is the jet Lorentz factor (the shock is assumed to be mildly relativistic). The local particle number density was expressed using the jet's equivalent isotropic power P_{iso} , which is related to the equivalent isotropic luminosity, $P_{iso} = L_{iso}/\epsilon_B$ (assuming radiative efficiency $\simeq \epsilon_B$, since in this model the magnetic energy is the primary cause for particle heating and radiation); L_{iso} is the equivalent isotropic luminosity. The estimated optical depth for absorption of IC photons is larger than unity at the early afterglow phase and yet much larger for internal shocks.

6 UPSTREAM MODIFICATION

The pairs produced through photon absorption in the upstream deposit energy and momentum, thus decelerating the plasma flow and decreasing the difference of Lorentz factors across the shock front. A quantitative treatment of this process is possible under the assumption that the flow is adiabatic, i.e., the energy and momentum of the newly born pairs are kept at the place of their birth and neither transported nor re-emitted. Let us consider two planes, parallel to the shock; one is infinitely close to the shock front (denoted 1) and the other is sufficiently far in the upstream (denoted 2), so that the IC radiation from the downstream is entirely absorbed between the planes. The upstream flow further away from the shock is undisturbed. In the quasi-stationary case,

the total energy and momentum between the planes is conserved; this means that their fluxes, taken at the two planes, must match each other. The corresponding equations read

$$w_1 \beta_1^2 \Gamma_1^2 + p_1 = w_2 \beta_2^2 \Gamma_2^2 + p_2 + S_{mom} \quad (22)$$

for momentum flux and

$$w_1 \beta_1 \Gamma_1^2 = w_2 \beta_2 \Gamma_2^2 - S_{en} \quad (23)$$

for energy flux. Here w is the specific enthalpy, p the pressure, Γ the bulk Lorentz factor, and β the bulk velocity divided by the speed of light. Equations (22) and (23) are nearly the same to those involved in the derivation of the Taub adiabat, except that their right-hand-side contains additional terms that take into account the energy and momentum flux densities, S_{en} and S_{mom} , carried by the IC radiation across plane 1.

It is convenient to introduce the following parametrization:

$$\begin{aligned} S_{en} &= a w_2 \beta_2 \Gamma_2^2 \\ S_{mom} &= b S_{en}. \end{aligned} \quad (24)$$

Here the absorption parameter a is the fraction of energy flux at the shock front, which is injected back into the upstream, while the parameter b is the ratio of momentum flux (multiplied by the speed of light) to the energy flux,

$$\int_0^{\pi/2} \cos \theta I(\theta) \sin \theta d\theta = b \int_0^{\pi/2} I(\theta) \sin \theta d\theta. \quad (25)$$

For a geometrically thin shock, $b \simeq 1/\Lambda \ll 1$.

We assume that the upstream acquires enough heat from pairs to guarantee a relativistic equation of state ($p_2 = w_2/4$) near the shock at plane 1, and that the shock is strong enough to make p_1 negligible. Then, the product $w_2 \beta_2 \Gamma_2^2$ can be obtained from Eq. (23) and substituted into Eq. (22), resulting in:

$$3\beta_2 + \frac{1}{\beta_2} = 4(1-a)\beta_1 - 4ab \equiv 4f, \quad (26)$$

where we introduce the feedback parameter f , which equals β_1 when there is no energy and momentum injection from the downstream to the upstream. Given that $(1-\beta_1)b \ll 1$, it is possible to eliminate b by introducing an effective absorption parameter $\tilde{a} = a(1+b)$, so that $f = (1-\tilde{a})\beta_1$. The roots of the above equation,

$$\beta_2 = \frac{2f \pm \sqrt{4f^2 - 3}}{3}, \quad (27)$$

correspond to the cases where the shock front is inside the region between the two planes (smaller value) or outside it (larger value, which is apparently the upstream velocity at the shock front). The smaller is the feedback parameter, the smaller is the upstream velocity at the shock front. There is a critical feedback parameter $f_{cr} = \sqrt{3}/2$, such that the discontinuity disappears; this happens already at a fairly small absorption parameter $\tilde{a}_{cr} \simeq 0.13$. If the efficiency of inverse Compton absorption is smaller than \tilde{a}_{cr} , then the upstream Lorentz factor at the discontinuity remains (at most) mildly relativistic down to $\tilde{a} \simeq 0.05$ and grows as $\Gamma_2 = 1/\sqrt{4\tilde{a}}$ in the limit $\beta_1 = 1, \tilde{a} \rightarrow 0$. The influence of pair loading on the upstream flow can be considered negligible only if $\tilde{a} \ll (2\Gamma)^{-2}$; for external shocks this is unreasonably small value. The bulk Lorentz factors at the shock as functions of the absorption parameter are presented in Fig. (2).

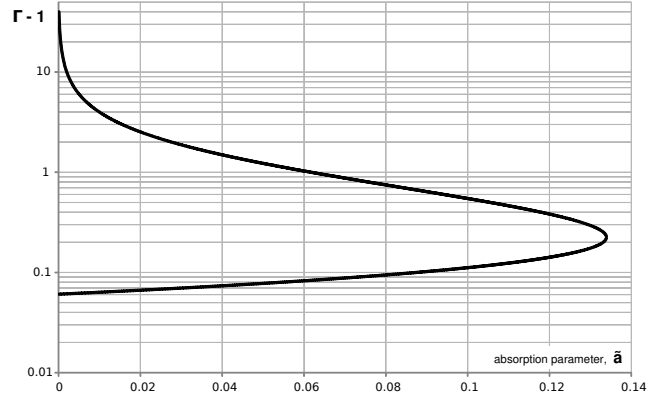


Figure 2. Bulk flow Lorentz factors in the shock-front comoving frame as functions of the effective absorption parameter \tilde{a} . The upper branch is for the upstream and the lower branch is for the downstream. The shock Lorentz factor is infinitely large.

Under realistic conditions, the pre-shock region cannot be fully adiabatic: the secondary pairs create turbulent magnetic field in the upstream that is growing towards the shock front, and the injected electrons eventually lose some energy either through synchrotron radiation, or through inverse Compton radiation in the radiation field of the shock. Radiative energy losses mean that the upstream is losing its inertia and it becomes more susceptible to deceleration, so that the upstream Lorentz factor at the discontinuity is smaller than in the adiabatic model.

An approximate solution for the upstream Lorentz factor (and then for energy density and electron distribution function) can be obtained if the equation of state for the upstream plasma is relativistic. This is satisfied for ultra-relativistic external shocks, where the upstream inevitably attains such an equation of state as it accelerates. This approximation may be less accurate for internal shocks that are only mildly relativistic. We assume that the equation of state for the upstream plasma is relativistic (this includes turbulent magnetic field), the momentum absorption parameter $b \ll (2/\sqrt{3} - 1)$, and we treat the absorption parameters $a = S_{en}/w\beta\Gamma^2$ and $b = S_{mom}/S_{en}$ as functions of the distance into the upstream (for example, the absorption parameters are the fraction of energy absorbed in the upstream from some distance up to infinity). Then, placing the two planes (1 and 2 mentioned earlier) infinitely close to each other, we obtain:

$$d \left(3\beta + \frac{1}{\beta} \right) = - \left(3\beta + \frac{1}{\beta} \right) d\tilde{a}. \quad (28)$$

The differentiated value in the left-hand-side has a minimum at $\beta = 1/\sqrt{3}$ (the relativistic speed of sound), so that \tilde{a} at this point should also have an extremum. Solving Eq. (28) for the upstream velocity in the shock-front frame, β , we obtain

$$\left(3\beta + \frac{1}{\beta} \right) = 4 \exp(-\tilde{a}). \quad (29)$$

Returning now to the solution of the original equations we note that the energy flux continuity (Eq. 23) and the proton number flux continuity yield

$$\frac{4}{3} e_{t,u} \beta \Gamma_u^2 (1-a) = \rho_0 c^2 \Gamma^2, \quad \beta \Gamma_u n = n_0 \Gamma, \quad (30)$$

where Γ_u is the upstream Lorentz factor relative to the shock front, $e_{t,u}$ the comoving-frame energy density, n the comoving number density of protons, ρ_0 the density of ambient medium, and n_0 its number density. In the region, where the upstream is highly relativistic both in the laboratory and in the shock frame, i.e., in the limit $\Gamma \gg \Gamma_u \gg 1$, equations (29) and (30) become

$$\Gamma_u = \frac{1}{2\tilde{a}^{1/2}}, \quad e_{t,u} = 3\Gamma^2 \rho_0 c^2 \tilde{a}, \quad n = 2\Gamma n_0 \tilde{a}^{1/2}. \quad (31)$$

Although these expressions do not provide explicit dependence on the distance to the shock front, they are sufficient to calculate the energy distribution of electrons injected into the downstream at the shock front.

7 PARTICLE INJECTION FROM THE UPSTREAM

The energy fed into the upstream, $e_{t,u}/n = (3/2)\Gamma m_p c^2 \tilde{a}^{1/2} \propto \Gamma_u^{-1}$ per proton, is due to injected electrons. Their comoving-frame energy is of the order of $\Gamma_u E_{ic}/2$ or larger (for those injected earlier), so that the number (per proton) of electrons injected with Lorentz factor γ_i or larger is $N(\gamma_i) \propto \gamma_i^{-2}$. After injection, the electrons gain energy as a result of flow compression, and, in the absence of radiative losses, their comoving-frame Lorentz factors grow as $n^{1/3}$. By the time an electron reaches the shock front, its Lorentz factor becomes $\gamma_f \sim \Gamma_u^{1/3} \gamma_i \propto \gamma_i^{4/3}$. Then, if all these electrons were able to keep their energy rather than radiate it away, the distribution of injected electrons at the shock front would be

$$N(\gamma_f) \propto \gamma_f^{-3/2}. \quad (32)$$

This distribution begins at $\gamma_f \sim \Gamma_{sh}^2 \gamma_{cr}/4$ and cuts off at $\gamma_f \sim \Gamma_{sh}^{4/3} \Gamma_{sh}^{2/3} \gamma_{cr}/4$, where Γ_{sh} is the upstream Lorentz factor at the shock front. The total injected power can be estimated as $(\Gamma_{sh}^2 \tilde{a})$ fraction of the shock power. For small absorption parameters, $\tilde{a} < 0.1$, this corresponds to a nearly constant fraction of 1/4.

The injection (32) represents the response of the upstream to the peak of downstream's IC radiation. It has a power-law tail and electrons from this tail produce high-energy IC radiation, extending well beyond the IC peak. These IC photons are absorbed again in the upstream and produce another generation of pairs. They are picked up by the relativistic (relative to the shock front) flow. When the pairs are brought back to the downstream, their energy is multiplied by a factor of at least Γ_{sh}^2 (up to $\Gamma_{sh}^{4/3} \Gamma_{sh}^{2/3}$ for a small number of pairs injected at the very beginning of the upstream acceleration), and they will produce even more energetic IC photons. This sequence of events starts the lepton cycle of converter acceleration Derishev et al. (2003), which – if not limited somehow – deposits almost all the available energy at the high-energy end of particle distribution, eventually leading to a cascade and formation of a nearly flat and featureless spectra³.

Our model avoids this problem. As a result of the

shock's self-tuning, the electrons, producing IC emission at its peak, radiate at the verge of Klein-Nishina regime and their Compton y parameter is of order unity. Thus, the efficiency of IC radiation decreases as electrons are accelerated and gain energy, and the converter acceleration becomes inefficient when the electrons' Lorentz factor satisfies the condition $\Gamma_{sh}^2 y(\gamma) < 1$. For this suppression mechanism to work, one needs that Γ_{sh} is not very large (implying a substantial upstream pair loading) and that the Compton y parameter rapidly decreases with increasing electron Lorentz factor (implying a paucity of low-frequency photons in the shock's spectrum that is achieved by heating in the downstream that efficiently eliminates low-energy electrons). In any case, the injection into the shock front of a very energetic electron population with a distribution given by Eq. (32) is an inevitable residue of the converter acceleration, which is always present if two-photon absorption opacity is not negligible. This population essentially produces a high energy transitional component in spectra, which we discuss in Sect. 11.

8 MAGNETIC FIELD GENERATION AND DECAY

At the moment of their creation in the upstream, the secondary pairs have anisotropic distribution. The recently injected pairs, whose momenta have not yet isotropized, can be considered as a “beam” in isotropic background plasma. The energy density of this beam is a small fraction $A \ll 1$ of the total energy density. The dominant contribution to the beam arises from the high-energy tail of IC spectrum, where the photons' absorption timescale is of the order of $t_{abs} = l_{abs}/c$ (not taking into account the difference of bulk Lorentz factors across the shock front, which, as we have shown above, is unlikely to be large). The more numerous less energetic pairs have a lower opacity and hence a lower injection rate. Consequently, their contribution to the anisotropic part of the distribution is less important.

The anisotropy of particle distribution function creates condition for the Weibel instability. For small anisotropy, its increment can be estimated as (Ruyer et al. (2015))

$$\Im \Omega \simeq A^{3/2} \omega_p. \quad (33)$$

The increment peaks at wavenumber

$$k_p \simeq A^{1/2} \omega_p / c, \quad (34)$$

which sets the spacial scale of the magnetic field in the upstream.

As the magnetic field grows, the isotropization timescale becomes smaller, that means smaller anisotropy and hence smaller increment. The growth of the magnetic field saturates when the increment becomes of the order of inverse injection timescale, that is

$$\Im \Omega \sim t_{abs}^{-1} \Rightarrow A \sim (t_{abs} \omega_p)^{-2/3}. \quad (35)$$

The saturated magnetic field is in equipartition with the beam of injected pairs Mart'yanov et al. (2008), so that the upstream magnetization is

$$\epsilon_{B,u} \sim A \sim \left(\frac{l_{s,u}}{l_{abs}} \right)^{2/3}, \quad (36)$$

³ It should be noted that in AGNs, where the jet's Lorentz factor is moderate, unrestricted converter acceleration may produce a reasonable outcome Stern & Poutanen (2008).

where $l_{s,u} = c/\omega_p$ is the skin length of the upstream plasma. This estimate suggests that as a consequence of the prolonged beam injection the upstream is only weakly magnetized, with $\epsilon_{B,u} \sim \text{few} \times 10^{-3}$ at most. On the contrary, anisotropy forms very fast at the shock front and the magnetic field at the downstream side is likely to be close to equipartition with the total energy density. Still this initial weak component is important as it produces large scale modes that eventually determine the rate of the magnetic field decay.

Estimating the anisotropy from Eq. 35 and substituting it into Eq. 34, we obtain the typical wavenumber for the magnetic field structures in the upstream

$$k_p \sim (l_{abs} l_{s,u}^2)^{-1/3}. \quad (37)$$

When amplified at the shock front, the long-wavelength modes have smaller increment, but they start from a finite seed amplitude, whereas the faster growing short-wavelength modes are dumped in the upstream to nearly vanishing amplitude. Thus, the amplified magnetic field at the shock front roughly preserves its spacial scale. For large-scale magnetic field perturbations it takes longer for the Weibel instability to develop and the shock front width increases by a large factor from standard the value $\sim l_s$ to $\sim (l_{abs} l_s^2)^{1/3}$, but still remains many orders of magnitude shorter than any other spacial scale. More importantly, the scale of perturbations determines how long the magnetic field survives in the downstream. Starting from the shock front and until the magnetic field spatial scale becomes extremely large, the magnetic field decay is governed by phase mixing and the decay length is $l_d \sim (k_p^3 l_{s,u}^2)^{-1}$ (see, e.g., [Chang et al. \(2008\)](#), but nonlinear corrections may increase the damping rate [Lemoine \(2015\)](#)), which agrees with our earlier assumption $l_d \sim l_{abs}$. Numerical simulations also show that in the case of long particle injection the magnetic field decay lasts for a time approximately equal to duration of the injection ([Garasev & Derishev \(2016\)](#)).

We do not derive the exact law of the magnetic field decay, but instead introduce two different models of the magnetic field decay. Model **I** describes exponential decay of the magnetic field, while model **II** is for a power-law decay:

$$\begin{aligned} \text{I. } B &= B_0 \exp(-r/l_d) & \Rightarrow & \gamma_0^2 \propto B^2 \\ \text{II. } B &= B_0 \left(\frac{1}{1+r/l_d} \right)^{1/q} & \Rightarrow & \gamma_0^2 \propto B^{2+q}. \end{aligned} \quad (38)$$

As shown in Sect. 10, different decay laws result in different low-frequency asymptotics of the downstream synchrotron emission.

9 SELF-TUNING

It is important to explore a self-regulating mechanism that arises naturally because of the downstream emission. The synchrotron SED around the peak is dominated by electrons that are close to the shock front. The peak is located at the energy $E_p \simeq \gamma_0^2(0) \hbar \omega_B$ (in the shock comoving frame). The value of $\gamma_0(0)$ (i.e., average Lorentz factor at the shock front)

can be obtained from Eq. (14). A simple estimate yields⁴:

$$\frac{16}{9\beta_d} \gamma_0^2(0) \sigma_T n_e (1 + \bar{y}_0) = \frac{1}{l_d}. \quad (39)$$

Substituting l_d from Eqs. (3) and (1) results in

$$E_p \simeq \frac{0.4 \epsilon_B^{1/2}}{\alpha_f \lambda (1 + \bar{y}_0) M} m_e c^2, \quad (40)$$

where α_f is the fine structure constant and $M = n_e/n_p$ the pair multiplicity. The latter is a free parameter, limited to $1 \leq M \lesssim m_p/m_e$, that takes into account possible pair loading. Given a bulk Lorentz factor $\Gamma \sim 300$, typical to GRBs, and an initial magnetic energy fraction $\epsilon_B \sim 0.1$, the product λM must be of the order of 10^4 for internal shocks and $10^6 \div 10^7$ for external shocks to fit the observations of the GRB prompt emission and early afterglow emission, respectively.

Now, consider a shock, whose pair multiplicity is $M = 1$ and λ is sufficiently small, so that $E_p \gtrsim m_e c^2 / \gamma_0$, i.e. the comptonization of the synchrotron radiation proceeds in the Klein-Nishina regime or close to it. We will show elsewhere that self-tuning can be reached also if this condition is not satisfied. However, in this paper we assume that it holds. In particular this condition is met in GRBs, both for external and internal shocks. In this case, the typical energy of the IC photons satisfies $E_{ic} \sim \gamma_0 m_e c^2$, enough to allow two-photon pair creation in collisions between synchrotron and IC photons, since $E_{ic} E_p \gtrsim (m_e c^2)^2$ ⁵. Given the Klein-Nishina suppression, the power of the IC emission relative to that of synchrotron emission is $P_{ic}/P_{sy} = \bar{y}_0/(1 + \bar{y}_0)$ and each electron in the downstream produces on average

$$M_{ph} \sim \frac{\bar{y}_0}{1 + \bar{y}_0} \frac{l_d}{l_c} \quad (41)$$

high-energy (inverse Compton) photons. After escaping from the shock front to the upstream, these photons may collide with synchrotron photons, producing electron-positron pairs.

The pairs are picked up by the plasma flow and are carried back to the shock. Thus, if M_{ph} exceeds one half, the pairs pile up in the shock, increasing the multiplicity M and reducing both the average Lorentz factor γ_0 and the energy of seed photons E_p . This leads to even greater inflow of secondary pairs to the shock, since the IC photons become less energetic (and more numerous, accordingly) and they interact with target photons that are closer to the cross-section maximum. The process continues until the product $E_{ic} E_p$ drops below $(m_e c^2)^2$, making pair production impossible for the bulk of IC photons. The pairs are also produced in the downstream, adding to the pair multiplication factor, but this is readily compensated by the self-tuning mechanism and thus has virtually no influence on the resulting spectrum.

Eventually, the shock reaches an attractor solution, where comptonization of synchrotron photons proceeds in

⁴ In this section we stick to the thermal distribution as a representative example. Power-law-type distributions result in a similar qualitative behavior and in numerical factors in the following equations.

⁵ Collisions between two IC photons can still produce pairs even if this condition is not met, but the efficiency is virtually negligible.

the Thomson regime (so that $E_{ic} = \gamma^2 E_p$) and internal absorption is efficient only for the high-energy tail of the IC spectrum. The contribution of the less numerous high-energy IC photons to the total number of secondary pairs produced at the shock may be relatively small. But these photons are absorbed quickly, as the shock opacity for them is defined by Eq. (19), and, because of their short life cycle, it is these photons that determine the pair multiplication increment, as well as the magnetic field build-up scale and strength.

At the attractor solution, the shock parameters will tune to make $\gamma_0(0) \simeq \gamma_{cr}$, where the critical electron Lorentz factor satisfies

$$\gamma_{cr} E_p = \gamma_{cr}^3 \hbar \omega_B = m_e c^2, \quad (42)$$

so that the rate of pair creation decreases. Solving this relation, we obtain

$$\gamma_{cr} = \left(\frac{B_{cr}}{B(0)} \right)^{1/3} \Rightarrow E_p \sim \left(\frac{2 L_{iso}}{B_{cr}^2 \Gamma^2 R^2 c} \right)^{1/6} m_e c^2, \quad (43)$$

where $B_{cr} \simeq 4.5 \times 10^{13}$ G is the Schwinger field strength. The lab-frame position of the synchrotron SED peak settles at

$$E_{p,lab} = \Gamma E_p \sim 400 \text{ keV} \times \frac{\Gamma^{2/3} L_{iso,51}^{1/6}}{R_{13}^{1/3}}. \quad (44)$$

This result is in remarkable agreement with the observed positions of SED peaks for both GRB prompt emission and the early afterglows. The tempting closeness of the prompt emission peak energy to $m_e c^2$, according to the proposed model of relativistic shock emission, is a mere coincidence, having its roots in the fact that the comoving-frame Lorentz factors of emitting electrons and the bulk Lorentz factor are of the same order.

The downstream region is also producing efficiently IC radiation that, as long as the shock is in the self-tuning regime, peaks at

$$E_{ic,lab} \sim \Gamma^2 \frac{(m_e c^2)^2}{E_{p,lab}} \sim 600 \text{ GeV} \times \frac{\Gamma^{4/3} R_{13}^{1/3}}{L_{iso,51}^{1/6}}. \quad (45)$$

However, there is no clear evidence for the second (high-energy) peak in the spectra of GRB prompt emission. This implies that an efficient absorption mechanism, which is unrelated to the proposed shock model and operates at energies down to 10-100 GeV must be active, somewhere near the prompt emitting region, for this model to fit observations. At the very early afterglow phase, the IC peak is expected to appear at somewhat higher energies (at or above 1 TeV) that are greatly attenuated by the interaction with the cosmic infrared background, so that its presence may be hard to observe.

During the later afterglow phase, expansion of the external shock eventually makes the optical depth for two-photon pair production too small to maintain the self-tuning of the shock. From this moment, the pair loading decreases and the electrons in the downstream increase their average Lorentz factor to maintain balance between the heating and the losses. This creates a feature in the lightcurve that is possibly related to plateau behavior, observed in some GRB afterglows (see, e.g., Nousek et al. (2006)). After the shock ends the self-tuning regime, the peak of IC emission shifts

to higher energies and its power drops because of the Klein-Nishina suppression.

10 THE DOWNSTREAM EMITTING REGION

A good proxy for the scale of the magnetic field build-up is the photon absorption length $l_{abs} = R/\Gamma\tau_c$. Using Eq. (19):

$$l_{abs} = \frac{E_p}{\sigma_{\gamma\gamma} e_B(0)} = \frac{4\sigma_T(1+\bar{y}_0)}{\sigma_{\gamma\gamma}} \frac{\gamma_0(0)E_p}{3\beta_d m_e c^2} l_c \sim 20 l_c. \quad (46)$$

Here e_B was taken from Eq. (5), Eq. 42 was used to substitute $\gamma_0(0)E_p$, and the numerical value for the two-photon pair production cross section used was $\sigma_{\gamma\gamma} = 10^{-25} \text{ cm}^2$ (close to the maximum). Given that the magnetic field dissipates on the same scale as it builds up, this guarantees that self-tuning automatically sets the shock in fast cooling regime.

We can turn now to estimate the spectrum of the emission produced in the downstream. For an isotropic electron distribution the synchrotron emission coefficient is

$$j_\omega(r) = \frac{\sigma_T n_e}{24\pi^2} \frac{m_e c^2}{e} B F_{tot} \left(\frac{2\omega}{3\gamma_0^2 \omega_B} \right), \quad (47)$$

where $\omega_B = eB/(m_e c)$ is the electron gyrofrequency and $F_{tot}(x)$ the dimensionless distribution-averaged emissivity function

$$F_{tot}(x) = \frac{1}{n_e} \int_0^\infty \bar{F} \left(\frac{\gamma_0^2 x}{\gamma^2} \right) f_e(\gamma, \gamma_0) d\gamma, \quad (48)$$

calculated using the distributions given in (11) or (12). Here we assume $\gamma_0 \gg 1$ in order to set the limit of the integral to 0 (instead of 1). The function $\bar{F}(x)$ is the emissivity function averaged over pitch angles

$$\bar{F}(x) = \int_0^{\pi/2} \sin^2(\phi) F \left(\frac{x}{\sin(\phi)} \right) d\phi. \quad (49)$$

Finally, we use the well-known expression Rybicki & Lightman (1979) for a single electron moving perpendicular to the magnetic field lines

$$F(x) = \frac{9\sqrt{3}}{8\pi} x \int_x^\infty K_{5/3}(\xi) d\xi, \quad (50)$$

where $K_{5/3}(\xi)$ is the modified Bessel function of the second kind. With our choice of numerical factor in Eq. (50), the normalization is

$$\begin{aligned} \int_0^\infty F(x) dx &= 1, & \int_0^\infty \bar{F}(x) dx &= \frac{2}{3}, \\ \int_0^\infty F_{tot}(x) dx &= \begin{cases} \frac{8}{9}, & \text{thermal distribution} \\ \frac{8(p-2)}{9(p-3)}, & \text{power-law distribution.} \end{cases} \end{aligned} \quad (51)$$

Fig. 3 depicts (with thin dashed line) the function j_ω for the thermal electron distribution. It's low-frequency asymptotic behavior, $F_{tot} \propto x^{1/3}$, is similar to that of functions F and \bar{F} . At high frequencies the thermal-averaged emission coefficient decays rather slowly, $F_{tot} \propto x^{5/6} \exp(-3x^{1/3}/2^{2/3})$, as compared to $\bar{F} \propto \exp(-x)$ and $F \propto \sqrt{x} \exp(-x)$. The function j_ω for the power-law distribution differs from its thermal counterpart in the high-energy tail, which in this case is also a power-law, $F_{tot} \propto x^{(1-p)/2}$.

The spectrum of the downstream synchrotron radiation can be obtained by integrating the emission coefficient along the shock normal⁶:

$$I_\omega = \Lambda \int_0^\infty j_\omega(B(r), \gamma_0(r)) dr. \quad (52)$$

For a given $B(r)$, we need to obtain $\gamma_0(r)$ before carrying out this integration. In general this cannot be done analytically and it must be solved numerically. However, if $\bar{y} \gg 1$ (this becomes increasingly accurate with a growing distance from the shock) we can advance further. Using $e_B \bar{y} \approx e_r(0)$ (that is accurate to a logarithmic factor, provided inverse Compton scattering is in the Thomson regime) we obtain a simple relation

$$\gamma_0^2 \propto \frac{\partial B^2}{\partial r}. \quad (53)$$

Using this relation, it is possible to integrate Eq. (52) numerically for any given $B(r)$. The inaccuracy in this approximate procedure results in underestimating the high-energy tail of the spectrum, and, consequently, this shifts the spectral maximum to a somewhat lower frequency.

The high-frequency asymptote of the integral spectrum is just the same as in the local emission coefficient, F_{tot} , because it is dominated by the most energetic electron population from the vicinity of the shock front. On the contrary, the resulting spectral index of the low-energy tail depends on the magnetic field decay law because the contribution of less energetic electrons from distant parts of the downstream may be important. To illustrate this, we calculate the synchrotron spectra for different magnetic field decay laws. The results are shown in Fig. 3 (for a thermal distribution) and Fig. 4 (for a distribution with a power-law tail with an index $p = 3.5$).

To reveal the low-frequency asymptote analytically, one may take a delta function instead of F_{tot} and then make use of the simple proportionality $\omega \propto \gamma_0^2 B$ and $dI \propto \gamma_0^2 B^2 dr$. In the case where ω , γ_0 and B , raised to appropriate powers, are all proportional to each other, we have

$$\omega I_\omega = \frac{dI}{d(\ln \omega)} \propto \frac{dI}{d(\ln B)} \propto \gamma_0^2 B^3 \left(\frac{\partial B}{\partial r} \right)^{-1} \propto B^4, \quad (54)$$

where B is to be substituted using Eq. 38 and the relation $\omega \propto \gamma_0^2 B$. A power-law magnetic field decay (model II) produces low-frequency asymptote $\omega I_\omega \propto \omega^{\frac{4}{3+q}}$, which is softer than the spectrum of an individual electron and approaches it only in the limit of $1/q \rightarrow \infty$ (the power-law decay becomes exponential in this limit). An exponential decay (model I) produces in this approximation the hardest possible low-frequency spectrum, $\omega I_\omega \propto \omega^{4/3}$, though a more accurate analysis reveals the asymptote $\omega I_\omega \propto \ln(\omega_p/\omega) \omega^{4/3}$, still slightly softer than for an individual electron.

⁶ Strictly speaking, one has to perform yet another integration over the local amplitude distribution of the turbulent magnetic field. However, this distribution is unknown and, for reasonable distributions, the integration affects only the distant part of the high-energy tail of the spectrum, which is of limited importance in any case. So, we avoid this unnecessary complication.

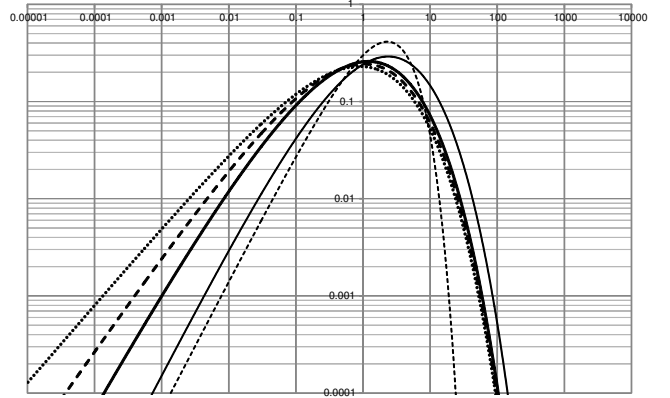


Figure 3. The spectral energy distributions (in arbitrary units) of the synchrotron radiation from the downstream region for a thermal distribution and for the different magnetic field decay models (see Eq. 38 in the text). Thick lines: model I (solid), model II with $q = 1$ (dashed), and model II with $q = 2$ (dotted). For comparison, we plot the spectral energy distributions produced in a uniform magnetic field by a thermal distribution (thin solid line) and by monoenergetic electrons with $\gamma = 1.4\gamma_0$ (thin dashed line). All spectra are normalized to have the same total power. The frequency (horizontal axis) is in units $\gamma_0(0)^2 \omega_B$.

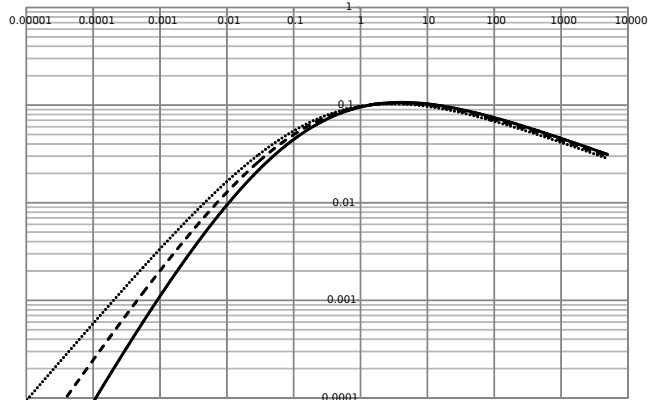


Figure 4. The spectral energy distributions of the downstream region synchrotron radiation for a power-law distribution with $p = 3.5$ and for different magnetic field decay models (see Eq. 38 in the text). Model I – solid line, model II with $q = 1$ – dashed line, and model II with $q = 2$ – dotted line. Same units and normalization as in Fig. (3) are used.

11 THE TRANSITIONAL RADIATION AND THE UPSTREAM EMITTING REGION

From the point of view of an individual electron, the upstream evolution looks as follows. When an energetic electron is produced, via pair creation far in the upstream, it finds itself in a rather weak magnetic field. Because of small magnetic field and strong Klein-Nishina suppression of IC radiation, it does not cool within the upstream dynamical timescale, but instead it gains energy due to adiabatic compression of the decelerating upstream flow. As time passes, the electron's comoving-frame Lorentz factor grows and so does the magnetic field strength around it. At the same time, the Lorentz factor relative to the shock's radiation field decreases, reducing the Klein-Nishina effect and increasing the energy losses due to IC. For the most energetic electrons,

the cooling timescale may eventually become comparable to the shock dynamical timescale. From this moment onwards, the evolution of the electrons' Lorentz factors resembles the standard “injection followed by fast cooling” scheme, where a power-law like spectrum is expected. This upstream emission component is due to a small number of secondary electrons injected at the time when the upstream fluid was not accelerated to relativistic velocity. The spectrum and the overall amplitude of this component are sensitive to details of the shock structure, which are beyond the scope of this paper. A unique feature of the upstream emission component is that it is produced in those regions of the upstream, which are close to the shock front and in which the bulk lab-frame Lorentz factor is large; it is just a few times smaller than that of the downstream. This emission that is roughly isotropic in the comoving frame, is beamed into a cone with a larger opening angle in the lab frame than the downstream emission. Thus this upstream emission component can be observed at larger angles and with a different temporal behavior compared with the downstream component originating from the same distance to the central engine.

The synchrotron cooling length for an electron in the upstream – given its low magnetization – is several orders of magnitude larger than the downstream cooling length, and the latter is only an order of magnitude shorter than the scale of magnetic field build-up (see Eq. 46). Under these circumstances, the synchrotron radiation is negligible for the bulk of secondary pairs in the upstream. However, those produced with Lorentz factors larger than $\gamma_c \sim \gamma_{cr} \epsilon_B l_c / (\epsilon_{B,u} l_{abs})$ will be in the fast cooling regime, provided the shock Lorentz factor is large enough to reach this limit at least early in the course of upstream acceleration. The inverse Compton radiative losses are marginally efficient for the bulk of secondary pairs. Since IC cooling proceeds in the Klein-Nishina regime, its net effect depends on the shape of synchrotron SED below the peak frequency. If this part of the spectrum is harder than $\nu F_\nu \propto \nu$, then IC cooling timescale increases with increasing electron Lorentz factor and the radiative losses in the upstream are not important for all electrons with $\gamma \ll \gamma_c$. In this case, the injected distribution (32) reaches the downstream largely intact. At the moment of shock crossing, the distribution of secondary pairs extends well beyond the equilibrium Lorentz factor $\gamma_0(0)$ and when they enter the downstream they quickly cool producing the transitional emission component, which was mentioned earlier. For realistic cases this distribution has a cutoff, which is more likely due to finite shock Lorentz factor, than due to cooling in the upstream. However, if the low-frequency asymptote of the synchrotron SED is softer than $\nu F_\nu \propto \nu$, then electrons with larger Lorentz factors have smaller IC cooling timescale. This redefines the cooling cutoff γ_c , decreasing it. In extreme case (very soft low-frequency asymptote) it becomes comparable to $\gamma_0(0)$ and the transitional component effectively disappears.

Whatever is the reason for the distribution (32) to cut off, it is nearly a power-law between $\Gamma_{sh}^2 \gamma_{cr} / 4$ and γ_c (effectively, $\gamma_c \sim \Gamma_{sh}^{4/3} \Gamma_{sh}^{2/3} \gamma_{cr} / 4$ if cooling is not important in the upstream). In the downstream, the injected electrons find themselves in the fast cooling regime if their Lorentz factor is larger than γ_{cr} and in a “fast heating” regime otherwise. The fast-cooling part of the injected electrons emits

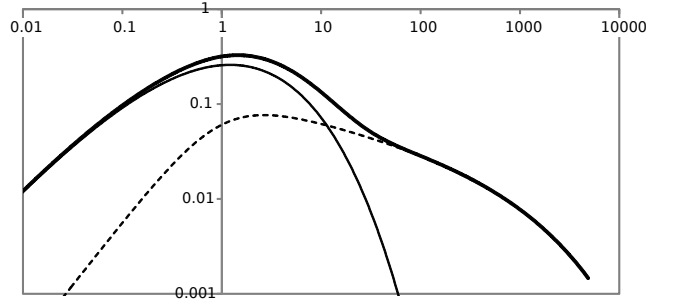


Figure 5. Composite synchrotron SED (thick solid line), resulting from superposition of emission from thermal downstream distribution (thin solid line, same as shown by thick solid line in Fig. (3)) and from fast-cooling injection at the shock front (schematically shown by thin dashed line). The cutoff Lorentz factor is $\gamma_c = 30\gamma_0(0)$ and normalization of the fast-cooling component corresponds to average Compton parameter $\bar{y} = 0.5$.

synchrotron radiation with the spectrum Derishev (2007)

$$\nu F_\nu \propto \frac{\gamma_f N(\gamma_f)}{1 + y(\gamma_f)} \propto \nu^{-1/4}, \quad (55)$$

where the synchrotron frequency is $\nu \propto \gamma_f^2$ and the Compton y parameter is small for electrons with $\gamma_f \gg \gamma_{cr}$. This slowly declining power-law spectrum extends from $\sim E_p$ to $\sim (\gamma_c/\gamma_{cr})^2 E_p$ and adds a high-energy tail to the shock's synchrotron SED even in the case where it is absent in the spectrum of the downstream emission. An example of such a composite spectrum is presented in Fig. (5).

12 DISCUSSION

We have presented a general self-consistent model for relativistic shocks with large compactness. Its natural applications are GRBs and AGNs, where one finds relativistic outflows and the compactness is high. The model allows us to calculate both the shock structure and the spectrum of its radiation. The model involves a relatively complex network of various processes, so that to explore it analytically we have to make some simplifying approximations and even introduce a phenomenological description at some points. Our analysis yields several important results. We list them here and briefly discuss how these results are related to GRB observations.

We have shown that the standard picture of collisionless shocks should be modified due to long range coupling between the upstream and the downstream. This coupling arises due to absorption in the upstream of IC photons produced at the downstream; it regulates and influences the structure of the shock. The shock has an intrinsic process of self tuning. As more and more pairs are produced in the upstream their multiplicity in the downstream increases reducing the typical synchrotron and IC energies until pair production in the upstream becomes marginal. Due to this self-tuning, the shock's parameters evolve toward an attractor solution in which the peak of the synchrotron SED is at such an energy that for an average radiating electron Comptonization proceeds close to the Klein-Nishina regime.

Due to the deposition of momentum by the IC photons in the upstream this region accelerates. The major change

in the Lorentz factor takes place in the upstream as it is gradually loaded with secondary pairs and the bulk Lorentz factor jump at the shock front is at most mildly relativistic even if the shock itself is ultrarelativistic (this makes the difference between GRB internal and external shock far less dramatic). At the same time, the downstream velocity appears to be considerably larger than the value $c/3$ found in unmodified shocks. The relatively small bulk Lorentz factor jump at the shock front combined with the Klein-Nishina suppression of the IC radiation at the high-energy tail of the electron distribution greatly diminish the efficiency of the converter acceleration discussed earlier and the shock avoids the unacceptable SEDs produced in this mechanism. The diffusive shock acceleration is also suppressed, because of the large downstream velocity, and it probably doesn't play any important role.

One of the most pronounced features of this model is that IC emission is approximately as efficient as synchrotron. This is an integral part of the model as these IC photons are those responsible for the self-tuning. There is no way to get rid of this IC peak within the model's framework. This emission is partially obscured from view by two-photon absorption within the shock itself, but the low-energy portion of the IC spectrum emerges unattenuated.

Unlike Blazars, GRBs don't have a prominent GeV second peak. With typical parameters this second peak is expected at around 100 GeV. While the limits on the prompt GRB spectra don't extend all the way to 100 GeV, it is clear that the lower energy ($\sim 1 \div 10$ GeV) tail of this component is not observed. The only way to resolve this discrepancy is to postulate the absorption of these high-energy photons close to the source. There are reasons for such an absorption in the high-compactness zone close to the central engine. The appearance of this second peak is not problematic for the external shock afterglow emission as in this case it is expected to be in the TeV range that is absorbed by the intergalactic IR background.

At the prolonged afterglow phase, the conditions change. Eventually the shocks become more and more transparent to IC radiation and at some point pair multiplication stops (gradually, rather than abruptly), the equilibrium electron Lorentz factor rises and so does the radiative efficiency in the synchrotron range. This compensates (or even overcompensates) for the effects caused by shock expansion and deceleration, thus producing a kind of plateau in the afterglow lightcurve. This predicted behavior may be related to the plateau feature observed in GRB afterglows. Despite the failure of self-tuning, the shock evolution after this point is still governed by the same set of physical processes and can be described with the help of our model. This analysis will be presented elsewhere.

The present model includes three distinct emitting regions with different spectra and evolution. Most of the emitted power comes from an extended region in the downstream with a declining magnetic field. Another emitting region is a thin layer next to the shock front, where energetic pairs advected from the upstream cool rapidly. This transitional region is responsible for the high-energy power-law tail in the observed spectra; it arises due to the converter acceleration. Finally, the most energetic electrons in the upstream cool radiatively. The most luminous part of the upstream region has a Lorentz factor lower than that of the downstream

and hence it has a broader beaming pattern and will have a different temporal pattern.

Turning to observations we note that there are indications that the observed spectra of GRB prompt emission can be decomposed into three components [Guiriec et al. \(2015\)](#), one of them looks like a thermal component, possibly a photospheric emission and the other two are presumably from optically thin regions, e.g. from internal shocks. If so, they may be related to the downstream and the transitional components in our model. Also, some afterglows show different behavior of optical and X-rays [Panaitescu et al. \(2006\)](#), which may be a signature of different emission components as well.

Finally we note that while the model has some promising features for the prompt spectra, such as the peak energy of the photons and the appearance of several different emission components, it does not resolve the so called "synchrotron line of death" problem. The low energy spectra are about as good in producing hard low-frequency asymptotes as it theoretically could be: under the right choice of parameters the low-frequency asymptote of shock's SED appears to be almost as hard as that of an individual synchrotron-emitting particle. However, some of the observed prompt GRB spectra violate this limit [Preece et al. \(2002\)](#). So there must be something more about the prompt phase, that is not captured by our model.

To conclude we note that the model proposed here offers a novel point of view on the physics of particle acceleration and magnetic field build up and decay in collisionless relativistic shocks. This model, which has never been explored before, ties together all the essential component of shock dynamics. The complexity of this model doesn't allow us to derive all its details here. Hence we explore only a particular implementation. The validity range of this implementation is rather broad, and in particular it is applicable to both prompt and afterglow GRB shocks. Still it does not cover all the interesting parameter space. In the future, other implementations of the same model framework will be explored, extending it to different regions in the parameter space with possible application to other astrophysical phenomena.

ACKNOWLEDGEMENTS

We thank Jonathan Katz for helpful comments. This research was supported in part by the Ministry of Education and Science of the Russian Federation under Contract No.14.Z50.31.0007, a RFBR grant 14-12-00766a, a CNSF-ISF grant 394/13, an ISA grant 3-10417, by the ISF-CHE I-Core center of excellence grant 1829/12 and by a JTF grant.

REFERENCES

- Ackermann M., et al., 2013, [ApJS](#), **209**, 11
- Bell A. R., 2004, [MNRAS](#), **353**, 550
- Beloborodov A. M., 2002, [ApJ](#), **565**, 808
- Beloborodov A. M., 2010, [MNRAS](#), **407**, 1033
- Blandford R. D., 1980, [ApJ](#), **238**, 410
- Chang P., Spitkovsky A., Arons J., 2008, [ApJ](#), **674**, 378
- Cohen E., Katz J. I., Piran T., Sari R., Preece R. D., Band D. L., 1997, [ApJ](#), **488**, 330
- Derishev E. V., 2007, [Ap&SS](#), **309**, 157

- Derishev E. V., Aharonian F. A., Kocharovsky V. V., Kocharovsky V. V., 2003, *Phys. Rev. D*, **68**, 043003
- Eichler D., 1979, *ApJ*, **229**, 419
- Garasev M., Derishev E., 2016, preprint, ([arXiv:1603.08006](https://arxiv.org/abs/1603.08006))
- Ghisellini G., Celotti A., Lazzati D., 2000, *MNRAS*, **313**, L1
- Gruber D., et al., 2014, *ApJS*, **211**, 12
- Gruzinov A., 2001, ArXiv Astrophysics e-prints,
- Guiriec S., et al., 2015, *ApJ*, **807**, 148
- Keren S., Levinson A., 2014, *ApJ*, **789**, 128
- Lemoine M., 2015, *Journal of Plasma Physics*, **81**, 014501
- Lyutikov M., Blandford R., 2003, ArXiv Astrophysics e-prints,
- Mart'yanov V. Y., Kocharovsky V. V., Kocharovsky V. V., 2008, *Soviet Journal of Experimental and Theoretical Physics*, **107**, 1049
- Medvedev M. V., Loeb A., 1999, *ApJ*, **526**, 697
- Medvedev M. V., Zakutnyaya O. V., 2009, *ApJ*, **696**, 2269
- Mészáros P., Rees M. J., 1997, *ApJ*, **476**, 232
- Milosavljević M., Nakar E., 2006, *ApJ*, **651**, 979
- Moiseev S. S., Sagdeev R. Z., 1963, *Journal of Nuclear Energy*, **5**, 43
- Murase K., Asano K., Terasawa T., Mészáros P., 2012, *ApJ*, **746**, 164
- Nousek J. A., et al., 2006, *ApJ*, **642**, 389
- Panaitescu A., Mészáros P., Burrows D., Nousek J., Gehrels N., O'Brien P., Willingale R., 2006, *MNRAS*, **369**, 2059
- Pe'er A., Mészáros P., Rees M. J., 2006, *ApJ*, **642**, 995
- Piran T., 2004, *Reviews of Modern Physics*, **76**, 1143
- Preece R. D., Briggs M. S., Mallozzi R. S., Pendleton G. N., Paciesas W. S., Band D. L., 1998, *ApJ*, **506**, L23
- Preece R. D., Briggs M. S., Giblin T. W., Mallozzi R. S., Pendleton G. N., Paciesas W. S., Band D. L., 2002, *ApJ*, **581**, 1248
- Ramirez-Ruiz E., Nishikawa K.-I., Hededal C. B., 2007, *ApJ*, **671**, 1877
- Rees M. J., Mészáros P., 2005, *ApJ*, **628**, 847
- Ruyer C., Gremillet L., Debayle A., Bonnaud G., 2015, *Physics of Plasmas*, **22**, 032102
- Rybicki G., Lightman A., 1979, *Radiative Processes in Astrophysics*. A Wiley-Interscience publication, Wiley, <https://books.google.ru/books?id=LtdEjNABM1sC>
- Ryde F., 2005, *ApJ*, **625**, L95
- Sari R., Piran T., Narayan R., 1998, *ApJ*, **497**, L17
- Sironi L., Spitkovsky A., Arons J., 2013, *ApJ*, **771**, 54
- Sironi L., Keshet U., Lemoine M., 2015, *Space Sci. Rev.*, **191**, 519
- Spitkovsky A., 2008a, *ApJ*, **673**, L39
- Spitkovsky A., 2008b, *ApJ*, **682**, L5
- Stern B. E., 2003, *MNRAS*, **345**, 590
- Stern B. E., Poutanen J., 2008, *MNRAS*, **383**, 1695
- Thompson C., Madau P., 2000, *ApJ*, **538**, 105

This paper has been typeset from a \LaTeX file prepared by the author.